**Disease Models & Mechanisms** 2, 359-373 (2009) doi:10.1242/dmm.002527
Published by The Company of Biologists 2009



# An ENU-induced mutation in mouse glycyl-tRNA synthetase (GARS) causes peripheral sensory and motor phenotypes creating a model of Charcot-Marie-Tooth type 2D peripheral neuropathy

Francesca Achilli[1], Virginie Bros-Facer[1,2], Hazel P. Williams[1], Gareth T. Banks[1], Mona AlQatari[3], Ruth Chia[1], Valter Tucci[6], Michael Groves[4], Carole D. Nickols[8], Kevin L. Seburn[9], Rachel Kendall[7], Muhammed Z. Cader[10], Kevin Talbot[10], Jan van Minnen[11], Robert W. Burgess[9], Sebastian Brandner[4,5], Joanne E. Martin[8], Martin Koltzenburg[2,3,5], Linda Greensmith[2,5], Patrick M. Nolan[6] and Elizabeth M. C. Fisher[1,5,*]

## SUMMARY

Mutations in the enzyme glycyl-tRNA synthetase (GARS) cause motor and sensory axon loss in the peripheral nervous system in humans, described clinically as Charcot-Marie-Tooth type 2D or distal spinal muscular atrophy type V. Here, we characterise a new mouse mutant, Gars$^{C201R}$, with a point mutation that leads to a non-conservative substitution within GARS. Heterozygous mice with a C3H genetic background have loss of grip strength, decreased motor flexibility and disruption of fine motor control; this relatively mild phenotype is more severe on a C57BL/6 background. Homozygous mutants have a highly deleterious set of features, including movement difficulties and death before weaning. Heterozygous animals have a reduction in axon diameter in peripheral nerves, slowing of nerve conduction and an alteration in the recovery cycle of myelinated axons, as well as innervation defects. An assessment of GARS levels showed increased protein in 15-day-old mice compared with controls; however, this increase was not observed in 3-month-old animals, indicating that GARS function may be more crucial in younger animals. We found that enzyme activity was not reduced detectably in heterozygotes at any age, but was diminished greatly in homozygous mice compared with controls; thus, homozygous animals may suffer from a partial loss of function. The *Gars$^{C201R}$* mutation described here is a contribution to our understanding of the mechanism by which mutations in tRNA synthetases, which are fundamentally important, ubiquitously expressed enzymes, cause axonopathy in specific sets of neurons.



## INTRODUCTION

The Charcot-Marie-Tooth (CMT) diseases (hereditary motor and sensory neuropathies) are the most frequent genetic disorders of the peripheral nervous system, affecting up to 1 in 2500 people (Skre, 1974). The CMT diseases are heterogeneous, manifesting with, among other features, distal muscle weakness and atrophy, and impaired sensation. One clinically useful grouping of CMTs is into primary demyelinating or axonal pathology. Demyelinating forms have a profound reduction in nerve conduction velocity (NCV), whereas CMTs resulting from primary axonal degeneration show normal, or slightly reduced, NCV but decreased amplitude of the compound muscle action potential or sensory nerve action potential (Antonellis et al., 2003). The hereditary motor neuropathies (HMNs) are related diseases involving degeneration of lower motor neurons, leading to muscle wasting. CMT type 2D (CMT2D) and distal spinal muscular atrophy type V (dSMAV/HMNV) are autosomal dominant disorders that generally result in slowly progressing weakness and atrophy, with focal wasting of the musculature.

Families segregating CMT2D and dSMAV were found to have causative mutations in the gene encoding glycyl-tRNA synthetase, *GARS* (Antonellis et al., 2003). GARS is an aminoacyl-tRNA synthetase: a group of evolutionary conserved enzymes that are essential for translation because they catalyse the addition of an amino acid to its cognate tRNA for protein synthesis. GARS is expressed ubiquitously and functions as a homodimer (Shiba et al., 1994; Williams et al., 1995).

Genetic and phenotypic screens have shown that different *GARS* mutations present a clinical continuum of predominantly distal motor neuronopathy/axonopathy with mild to moderate sensory loss, varying within and between families (Sivakumar et al., 2005; Del Bo et al., 2006; Dubourg et al., 2006; James et al., 2006). Typically, the first symptom is muscle weakness in the hands, which develops at between 8 and 36 years of age; the involvement of the lower extremities varies.

Seburn and colleagues reported the mouse mutant Gars$^{Nmf249}$; these mice have severe sensory and motor axonal neuropathy, and die by 6-8 weeks of age (Seburn et al., 2006). *Gars$^{Nmf249/+}$* mice have abnormal neuromuscular junctions and muscle force. They have

[1]Department of Neurodegenerative Disease, [2]Sobell Department of Motor Science and Movement Disorders, [3]Institute of Child Health, [4]Division of Neuropathology, [5]MRC Centre for Neuromuscular Diseases, Institute of Neurology, University College London, London WC1N 3BG, UK
[6]MRC Mammalian Genetics Unit, [7]MRC Mary Lyon Centre, Harwell, Didcot, Oxfordshire OX11 0RD, UK
[8]Department of Histopathology, Queen Mary University of London, London E1 1BB, UK
[9]The Jackson Laboratory, Bar Harbor, MA 04609, USA
[10]MRC Functional Genetics Unit, Department of Physiology, Anatomy and Genetics, University of Oxford, Oxford OX1 3QX, UK
[11]Department of Cell Biology and Anatomy, Hotchkiss Brain Institute, University of Calgary, Calgary, Alberta T2N 4N1, Canada
*Author for correspondence (e-mail: e.fisher@prion.ucl.ac.uk)

reduced nerve conduction velocities, with a loss of large diameter peripheral axons, but no myelination defects. A loss-of-function allele, *Gars*$^{XM256}$, resulting from a gene-trap insertion, shows no dominant phenotype; therefore, the Gars$^{Nmf249}$ phenotype is not caused by a simple haploinsufficiency and may result from a gain of function (Seburn et al., 2006).

In this study, we report a new mouse mutant, Gars$^{C201R}$, which gives rise to a less severe phenotype than Gars$^{Nmf249}$, and which has locomotor and sensory deficits. Heterozygous animals show reduced grip strength that is modulated by genetic background, a reduction of axon diameter in peripheral nerves, slowing of nerve conduction and an alteration in the recovery cycle of myelinated axons; altered muscle characteristics and innervation are also seen, although these are no obvious defects in the motor neurons. We are able to produce homozygous mice, but these mice die by postnatal day 17 with gait disturbance, loss of large diameter axons and other neurological changes. GARS enzyme activity in the brains of *Gars*$^{C201R/+}$ mice is not significantly different from in wild-type mice but, unexpectedly, is reduced by 60% in the homozygotes when compared with wild-type controls. The Gars$^{C201R}$ mouse is a valuable resource that provides an insight into the mechanism of axonopathy resulting from mutations in this ubiquitously expressed aminoacyl-tRNA synthetase.

## RESULTS

### Origin of Gars$^{C201R}$ mice and phenotype on two genetic backgrounds

Two male F1 (C3H × BALB/c) mice were identified during a routine screen in a large ENU (*N*-ethyl-*N*-nitrosourea) mutagenesis project at the Medical Research Council (MRC) Mammalian Genetics Unit (Nolan et al., 2000). The animals were siblings, F1 progeny of a BALB/cAnN G0 mutagenised male crossed to a C3H/HeH female, and had deficits in grip strength, locomotor activity and rotarod when screened using the SHIRPA protocol at 6 weeks of age (data not shown) (Rogers et al., 1997; Rogers et al., 2001). Frozen sperm from each sibling was used for in vitro fertilisation of C3H/HeH females to produce a set of offspring (termed the N2 progeny) from each F1 male; the litter sizes were *n*=19 and *n*=26.

Based on the SHIRPA results from the founder siblings, we adopted grip strength as a robust score for 'affected' and 'unaffected' status in the N2 mice and following generations (Rogers et al., 1997). Because the cohorts of affected progeny of each sibling showed no significant phenotypic differences from each other, and because these cohorts were subsequently shown to carry the same mutation, from here on we combine all progeny data into cohorts either with the '*Gars*$^{C201R}$' mutation or without the mutation (the 'wild-type littermate control' cohort). After the *Gars*$^{C201R}$ mutation had been identified, the mutation status for all animals was confirmed subsequently by genotyping. We bred the N2 progeny either by backcrossing to C3H/HeH mice to create N3 and N4 animals, or by backcrossing to C57BL/6J mice to create N1 and N2 mice. All of the assays discussed here took place using these N3/N4 (C3H) or N1/N2 (C57BL/6) cohorts, unless stated otherwise. Heterozygous animals on both genetic backgrounds appear to have a normal life span (living to at least 17 months of age).

The grip strength of all four limbs combined was assessed longitudinally from 1-15 months of age. Animals were also weighed and no significant differences in weight were seen between heterozygous and wild-type animals with the same genetic background (i.e. within either the N3/N4 C3H or N1/N2 C57BL/6 cohort). From 1-15 months of age, a significant reduction in grip strength was seen in both male and female *Gars*$^{C201R/+}$ mice compared with sex-matched wild-type littermates on both C3H and C57BL/6 backgrounds (Fig. 1; supplementary material Fig. S1). For example, the mean grip strength of 3-month-old *Gars*$^{C201R/+}$ males on the C3H background (*n*=11) was 123.9±7.4 units compared with 205.5±6.3 units in male littermate controls (*n*=10), an average reduction of 40%. However, the phenotype was considerably more pronounced on the C57BL/6 background than the C3H genetic background. At 3 months of age, the mean grip strength of *Gars*$^{C201R/+}$ males on the C57BL/6 background (*n*=23) was 75.4±3.7 units compared with 177.1±7.5 in wild-type littermates controls (*n*=14), a reduction of 57%. This indicates that genetic modifiers segregating between the C3H/HeH and C57BL/6J backgrounds are having a pronounced effect on phenotype.

The motor phenotype of *Gars*$^{C201R/+}$ mice was defined further by measuring performance in an assay for skilled motor function, the mouse reaching and grasping test (MoRaG) (Tucci et al., 2007); this test is used to assay fine motor control because in many species, including the mouse, the capacity to modulate a motor pattern according to the task is essential for adaptation to the environment. MoRaG is used to assess forepaw reaching and grasping motor phenotypes: briefly, over a number of sessions, mice are trained to reach through a narrow opening with their forepaws to retrieve food pellets. MoRaG revealed differences between *Gars*$^{C201R/+}$ males (*n*=9) and wild-type littermate controls (*n*=10) (with the C3H background). Quantitative analysis showed a statistically significant increase ($P<0.05$) in the latency to the first reaching (LFR), an indication of decreased motor flexibility. Furthermore, the percentage of errors in grasping food pellets was approximately 40% higher in *Gars*$^{C201R/+}$ mice compared with control mice; this difference was evident in the first session and sustained (more than 30% higher) during the second session (Fig. 1D-F). In the first session, no significant difference in the accuracy in reaching the target was observed between the two groups. However, in the second session, the wild-type group showed a reduction in percentage errors, an index of motor improvement, whereas *Gars*$^{C201R/+}$ mice maintained a low performance in both sessions. Thus, the *Gars*$^{C201R/+}$ mice have decreased motor flexibility and a diminution in fine motor control.

### Homozygous *Gars*$^{C201R/C201R}$ mice

We carried out intercrosses of the *Gars*$^{C201R/+}$ mice on both the C3H and C57BL/6 backgrounds, generating N5/N6 and N3/N4 mice, respectively. The C3H background (the milder phenotype) produced seven *Gars*$^{C201R/C201R}$ mice out of a total of 60 progeny (12%); the C57BL/6 background produced four *Gars*$^{C201R/C201R}$ mice out of a total of 76 progeny (5%). Owing to unknown reasons, all homozygous *Gars*$^{C201R/C201R}$ mice died by postnatal day 17 on the C3H background and by day 15 on the C57BL/6 background. A comparison of the weights of three male C3H homozygotes at 15 days of age showed an average weight of 3.1 grams compared with an average of 8.0 grams in their male wild-type and heterozygote littermates, a decrease of 61%. Homozygous animals were distinguishable early on by their small size and greatly impaired limb movement; this was so severe in some cases that animals were culled

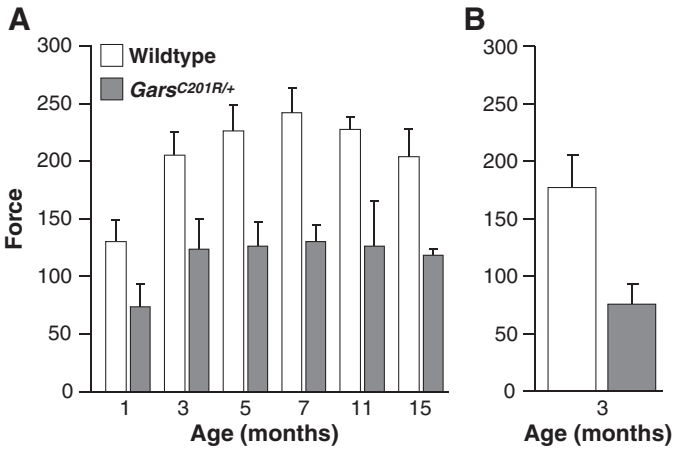


C

| | | Male | Female |
|---|---|---|---|
| C3H | Wildtype | 206±6 (n=10) | 167±7 (n=7) |
| | *Gars*$^{C201R/+}$ | 124±7 (n=11) 60% | 111±3 (n=9) 67% |
| C57BL/6 | Wildtype | 177±8 (n=14) | 166±45 (n=19) |
| | *Gars*$^{C201R/+}$ | 75±4 (n=23) 42% | 71±3 (n=24) 43% |

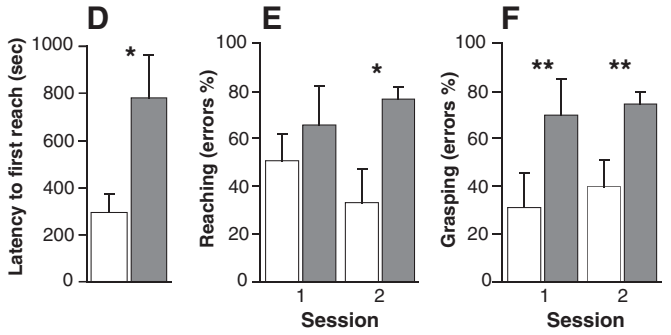


**Fig. 1. Motor deficits in *Gars*$^{C201R/+}$ mice.** Four-paw grip strength of *Gars*$^{C201R/+}$ male mice compared with sex-matched wild-type littermates. (A) Mice with a C3H genetic background from 1 to 15 month of age. The numbers of mice sampled varied with the time point: *Gars*$^{C201R/+}$, *n*=5-11; wild-type littermates, *n*=4-10. (B) Mice with a C57BL/6 background at 3 months of age: *Gars*$^{C201R/+}$, *n*=23; wild-type littermates, *n*=14. (C) Mean grip strength values (units) for *Gars*$^{C201R/+}$ and wild-type littermates at 3 months of age on the C3H and the C57BL/6 genetic backgrounds. The average value of the heterozygote grip strength is also shown as a percentage of its wild-type littermate control cohort. (D-F) Reaching and grasping deficits in *Gars*$^{C201R/+}$ male mice (*n*=9) compared with sex-matched wild-type littermates (*n*=10), as detected by the MoRaG test. (D) The latency to the first reach (LFR) is the response time for reaching within the first session; the percentages of errors during reaching (E) and grasping (F) are shown for *Gars*$^{C201R/+}$ and wild-type controls. Levels of statistical significance are: **P*<0.05 and ***P*<0.01.

a few days after birth, according to UK animal welfare regulations, because they were unable to move to suckle (supplementary material Movies 1 and 2). Whole-mount neurofilament staining did not show any obvious abnormalities in the peripheral nervous system of heterozygotes at 12.5 days post coitum (dpc) (C. Ruhrberg, personal communication); we have not looked at homozygotes.

### Identification of the *Gars*$^{C201R}$ mutation

We undertook a candidate positional cloning approach to identify the mutant locus. As both founder siblings and their progeny had indistinguishable phenotypes on all of the tests carried out, they probably carried the same mutation; nevertheless, there was a formal possibility that different mutations could have arisen either in the G0 BALB/c male and/or in the C3H female to which this male had been crossed.

We carried out a genome scan, on the C3H background, with 13 affected N2 progeny from each of the two F1 siblings: 72 polymorphic genome-wide single-nucleotide polymorphisms (SNPs) were genotyped and linkage was found to mouse chromosome (Mmu) 6 at between 22 and 114 Mb, and 22 and 84 Mb, respectively (data not shown). To refine the mapping and reduce the critical region, haplotype mapping of 61 and 29 affected mice from each sibling cohort was carried out and recombinant chromosomes indicated that the mutation must lie between 53 and 73 Mb, and 53 and 58 Mb, respectively. This region has homology to human chromosome 7p15, which contains the *GARS* gene; the mouse ortholog maps to 55 Mb on Mmu 6 [see the Online Mendelian Inheritance in Man (OMIM) website, www.ncbi.nlm.nih.gov].

Of the many candidate genes in the region, the *Gars* gene stood out because mutation of this gene in humans can give rise to locomotor deficits, as we described in the mice. Therefore, we sequenced the mouse *Gars* gene and found a point mutation in a BALB/c haplotype in exon 5. In both cohorts, the point mutation was a T to C transition at base pair 456 that results in a non-conservative cysteine to arginine substitution at residue 201. Thus, the mutant phenotype of the founder siblings was almost certainly derived from the same ENU-induced mutation as in their BALB/c father. The mutation was designated *Gars*$^{C201R}$ and was not present in BALB/c, C3H, C57BL/6 or any other strain sequenced, including 129/J, A/J, AKR/J, CD1, DBA/2J, FVB/J, LP/J, MOLF, NZW, PWK, RIIIS, SJL, SM/J, SWR and VM.

Intercrossing heterozygous *Gars*$^{C201R/+}$ mice with heterozygous *Gars*$^{XM256/+}$ mice (the loss-of-function gene trap allele) yielded a total of 40 progeny with three of the expected genotypes (wild-type, *Gars*$^{C201R/+}$ and *Gars*$^{XM256/+}$); however, the fourth expected genotype, double heterozygotes (*Gars*$^{C201R/XM256}$), was absent, indicating non-complementation of the two alleles and embryonic lethality, thereby providing evidence that the *Gars*$^{C201R}$ mutation is causative for the phenotype.

This mutation at residue 201 lies within the highly conserved catalytic domain of the protein and potentially within the acceptor stem recognition site (Fig. 2) (Xie et al., 2007). This cysteine residue is conserved across a diverse range of organisms from humans to Drosophila and Arabidopsis (Fig. 2A). The *Gars*$^{C201R}$ mutation creates a restriction enzyme digestion site for the enzymes *Hae*II and *Hha*I, enabling a protocol to be designed for routine genotyping using PCR and restriction fragment length polymorphism (RFLP) analysis (see Methods). All animals that had previously been scored as affected were genotyped and shown to carry the mutation; all unaffected mice were wild-type at this locus.

### GARS protein levels and enzyme activity

GARS protein expression levels were examined by probing western blots of the homogenate of a standardised dissected portion of brain that included the motor and sensory cortex (Fig. 3A). Homogenates were made from wild-type, *Gars*$^{C201R/+}$ and *Gars*$^{C201R/C201R}$ mice at 15 days of age on the C3H background, and from wild-type and

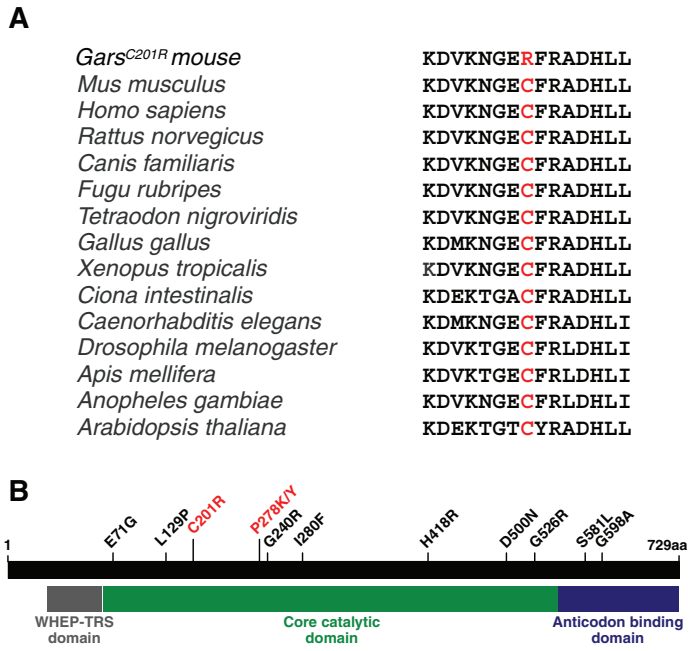


**Fig. 2. The GARS protein.** (A) The mutated residue in the Gars$^{C201R}$ mouse is highly conserved from mammals through to Arabidopsis. (B) Known mutations in humans (in black) and mice (in red) are scattered throughout the GARS protein; the mouse mutation marked as P278K/Y is the *Gars*$^{Nmf249}$ mutation reported by Seburn and colleagues (Seburn et al., 2006). Note that there are discrepancies in the numbering of mutations in humans and mice – the protein shown here is the full-length mouse protein (Ensembl peptide ID ENSMUSP00000003572), which is the mitochondrial GARS; the cytosolic protein is shorter because it starts with an internal ATG. The mouse mutations are numbered according to the full-length form of the protein, whereas the human mutations are numbered according to the cytosolic form (Seburn et al., 2006). The *Gars*$^{C201R}$ mutation lies within the catalytic domain, as described by Schimmel and colleagues (Xie et al., 2007).

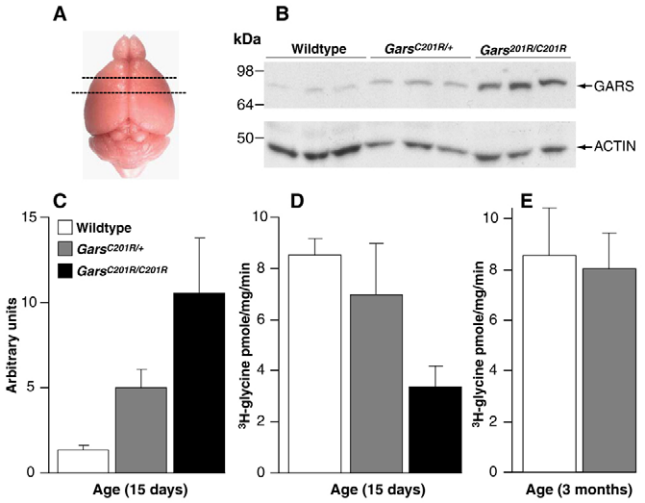


**Fig. 3. GARS anomalies in the Gars$^{C201R}$ mouse brain.** Protein levels and enzyme activities of GARS in dissected brain homogenates from wild-type, *Gars*$^{C201R/+}$ and *Gars*$^{C201R/C201R}$ mice at 15 days of age ($n$=3 for each cohort) and from wild-type and *Gars*$^{C201R/+}$ mice at 3 months of age ($n$=3 for each cohort); all mice were on the C3H background. (A) The dissected region, within the dotted lines, of 15-day- and 3-month-old *Gars*$^{C201R/+}$ and wild-type littermate brains, which includes the motor and sensory cortex (mouse atlas, www.mbl.org/). (B) Western blot showing levels of GARS protein in wild-type, heterozygous and homozygous littermates at 15 days of age. (C) Graph of quantified data from the western blot, normalised to the β-actin control. (D,E) Acylation activity of GARS in brain homogenates. (D) GARS activity in homogenates of the dissected motor and sensory cortex of wild-type, heterozygous and homozygous littermates at 15 days of age, and (E) wild-type and heterozygotes at 3 months of age.

*Gars*$^{C201R/+}$ mice at 3 months of age on the C3H and C57BL/6 backgrounds. Western blots of these homogenates were probed with an antibody to mouse GARS. The membrane was then stripped and reprobed with an antibody to β-actin as an internal protein loading control. The signal from the autoradiograph bands was quantified and the GARS levels normalised for β-actin (Fig. 3B,C). At 3 months, there was no significant difference in GARS levels between wild-type and *Gars*$^{C201R/+}$ brain homogenates in either genetic background (supplementary material Fig. S2). However, at 15 days of age, there were significant increases in protein levels in both heterozygotes and homozygotes compared with wild-type littermates (Fig. 3C). Heterozygotes showed an increase of 3.8-fold compared with wild-type mice ($P$=0.014) and homozygotes showed an increase of 8.2-fold compared with the wild-types ($P$=0.034).

To investigate the possible molecular mechanisms of pathology, GARS aminoacylation activity was assayed directly in homogenates of the same dissected portion of brain from wild-type, *Gars*$^{C201R/+}$ and *Gars*$^{C201R/C201R}$ mice on the C3H background at 15 days of age (N5/N6 generation), and from wild-type and *Gars*$^{C201R/+}$ mice on both C3H (N5/N6) and C56BL/6 (N3/N4) backgrounds at 3 months of age. Assays were carried out blind to the genotype, which was decoded afterwards.

The enzyme functions as a homodimer and, in our assay, we found that GARS aminoacylation activity was not significantly different between wild-type and heterozygous C3H mice at 15 days and 3 months of age (Fig. 3D,E). However, the mean GARS activity in 15-day-old C3H *Gars*$^{C201R/C201R}$ mice ($n$=3) was 3.4±0.8 pmole/mg/minute and thus was reduced by 60% in comparison with the mean value of 8.5±0.4 pmole/mg/minute for wild-type littermate controls ($n$=3) ($P$=0.01) (Fig. 3D). GARS activity was not significantly different between wild-type and *Gars*$^{C201R/+}$ mice on the C57BL/6 background at 3 months of age (data not shown).

### General histopathology

Haematoxylin and eosin (H&E)-stained sections of various tissues were examined in the C3H background in three wild-type and six heterozygote littermates at 17 months of age, and in two wild-types, two heterozygotes and two/three homozygotes at 15 days of age. No abnormalities were observed in the heart, lung, liver, kidney, adrenal glands, skin or gut, although organ size was reduced (in proportion to body size) in homozygotes compared with in heterozygous and wild-type littermates.

Brain and spinal cord sections were stained with H&E, Luxol Fast Blue-Cresyl Violet, and for glial fibrillary acidic protein and choline acetyl transferase. No abnormalities, including

demyelination or inflammation, were seen in heterozygous animals at 17 months or 15 days of age.

In cross sections of 17-month-old $Gars^{C201R/+}$ sciatic nerves ($n$=3), we found a 50% reduction in the number of large diameter axons compared with in wild-type littermates ($n$=3) ($P$=0.03) (supplementary material Fig. S3A). To investigate potential motor and/or sensory involvement, we went on to analyse a cohort of heterozygous 3-month-old $Gars^{C201R/+}$ mice with a C57BL/6 background and their wild-type littermates.

### Assessment of hindlimb muscle force and muscle contraction characteristics, and motor unit and motor neuron survival

In order to examine whether motor pathways were affected in $Gars^{C201R/+}$ heterozygotes, an in vivo physiological analysis of muscle and motor function, and a morphological analysis of hindlimb muscles and motor neuron survival were performed in adult female $Gars^{C201R/+}$ heterozygotes and sex-matched wild-type littermate controls. The mice were examined at 4 months of age (120 days), with a cohort size of $n$≥5 per cohort on the C57BL/6 background (N3/N4 generation). Each animal was weighed and, by 120 days of age, female $Gars^{C201R/+}$ heterozygote mice weighed an average of 20.7±1.1 grams, which is significantly less than their female wild-type littermates, which had an average weight of 23.5±0.6 grams ($P$=0.005). Thus, as the animals become more inbred onto the C57BL/6 background, we see an effect on body weight that is not significant in the more mixed background of the N1/N2 generation, which was used for grip strength analysis.

To assess muscle force, we examined the maximum force of the two hindlimb muscles: the tibialis anterior (TA) and the extensor digitorum longus (EDL). In $Gars^{C201R/+}$ mice, the TA had a maximum twitch of 20.7±0.8 grams; this was significantly weaker than the TA muscle force in wild-type littermates, which had a maximum twitch force of 36.1±1.8 grams ($P$<0.001) (Fig. 4A). The maximum tetanic force of TA muscles in $Gars^{C201R/+}$ mice was also significantly less than that in wild-type littermates, with the TA muscles in $Gars^{C201R/+}$ mice producing only 67.1±1.9 grams compared with 125.1±2.8 grams in wild-type littermates ($P$<0.001) (Fig. 4B). However, there was no significant difference in the force output of the EDL muscles in $Gars^{C201R/+}$ mice compared with wild-type littermates. The EDL muscles of the $Gars^{C201R/+}$ mice produced a maximum twitch of 7.57±0.4 grams compared with 9.31±0.7 grams in wild-type littermates, and a maximum tetanic force of 21.8±1.2 grams compared with 24.6±1.7 grams in wild-types (data not shown). Interestingly, we found that in the $SOD1^{G93A}$ mouse model of amyotrophic lateral sclerosis (ALS), both the TA and EDL are equally and severely affected by the end stage of the disease, whereas the TA is affected more profoundly at the earlier stages of the disease (Sharp et al., 2005). Therefore, it is possible that the first signs of muscle wasting in $Gars^{C201R/+}$ mice appear in TA muscles and that they may be indicative of the appearance of late-onset motor neuron pathology.

The preservation of force in the EDL muscles could be the result of more efficient reinnervation by the remaining motor axons following loss of connectivity, or it could simply be the result of milder or non-existent denervation in this muscle compared with the TA. In order to assess whether there were any physiological signs of motor neuron degeneration in $Gars^{C201R/+}$ mice, we assessed the number of functional motor units that were

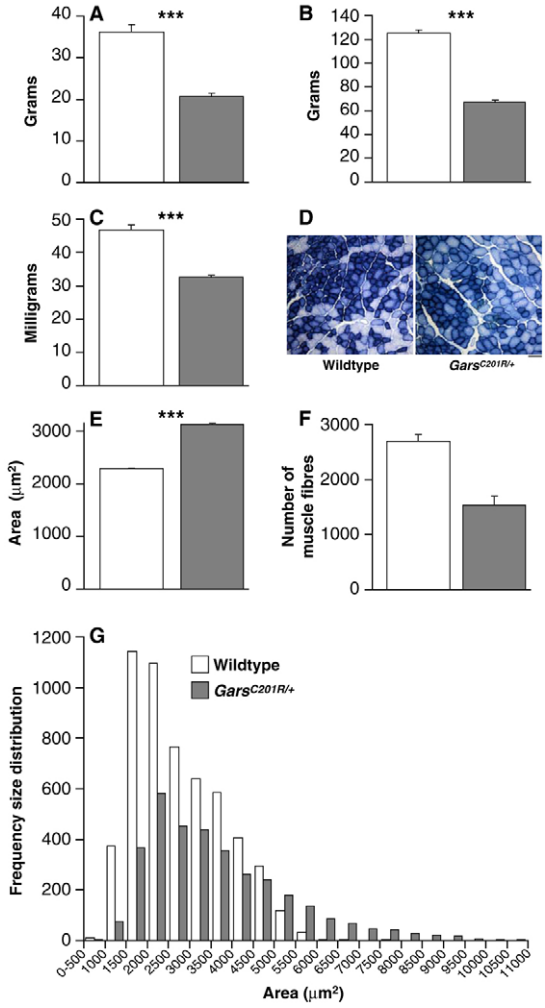


**Fig. 4. Maximum TA muscle force and histopathological analysis of muscle fibres in 4-month-old wild-type and $Gars^{C201R/+}$ mice.** The maximum twitch (A) and tetanic (B) force (grams) generated by TA muscles from wild-type ($n$=10) and $Gars^{C201R/+}$ ($n$=10) littermates (***$P$<0.001). (C) The weight of TA muscles from wild-type ($n$=10) and $Gars^{C201R/+}$ ($n$=10) littermates (***$P$<0.001). (D) Examples of TA muscle sections, stained for succinate dehydrogenase, an indicator of oxidative capacity, from (left) wild-type and (right) $Gars^{C201R/+}$ mice. Bar, 70 μm. Histograms representing the mean size of cross-sectional areas of TA muscle fibres (E) (***$P$<0.001) and the mean number of TA muscle fibres (F) from wild-type ($n$=3) and $Gars^{C201R/+}$ ($n$=3) littermates. Errors bars represent the standard error of the mean (s.e.m.). The data collected on muscle fibre sizes were sorted into frequency distribution histograms (G).

innervating the EDL muscles in $Gars^{C201R/+}$ mice by stimulating the sciatic nerve with electrical impulses of increasing intensity. Representative examples of motor unit traces from the EDL muscles of wild-type and $Gars^{C201R/+}$ mice are shown in supplementary material Fig. S4A,B, respectively, and the mean motor unit survival in each group is summarised in supplementary material Fig. S4C.

We found no evidence of motor unit loss in 4-month-old $Gars^{C201R/+}$ mice, with an average of 39±1 motor units innervating the EDL of $Gars^{C201R/+}$ mice compared with an average of 37±1 motor units in the EDL muscles of the wild-type mice; this

difference was not significant. We also examined whether the phenotype of the EDL muscles was altered in *Gars*$^{C201R/+}$ mice. EDL muscles are normally fast muscles that fatigue rapidly when stimulated repeatedly (see supplementary material Fig. S4D). We established the response of EDL muscles to repetitive stimulation in 120-day-old wild-type and *Gars*$^{C201R/+}$ mice and found that the responses were not significantly different (supplementary material Fig. S4D,E, respectively). Furthermore, there was no change in the fatigue index (F.I., the maximum muscle force at the end of a 3-minute period of stimulation, expressed as a ratio of the maximum force at the start of the test) of the EDL in *Gars*$^{C201R/+}$ mice, which had an F.I. of 0.77 compared with 0.74 in wild-type littermates (supplementary material Fig. S4F), where an F.I. value approaching 1 indicates that a muscle is highly fatigable.

At the end of the physiological tests, the hindlimb muscles from *Gars*$^{C201R/+}$ mice and their wild-type littermates were removed and weighed. The results showed that the muscle weakness observed in *Gars*$^{C201R/+}$ TA muscles was reflected in a significant reduction in weight, so that TA muscles from *Gars*$^{C201R/+}$ mice weighed on average 32±0.64 milligrams compared with 46±1.48 milligrams in wild-type mice ($P$<0.001) (Fig. 4C). TA muscles were also stained for succinate dehydrogenase (SDH) activity. As shown in Fig. 4D, a greater proportion of muscle fibres stain darkly for SDH in *Gars*$^{C201R/+}$ mice compared with control TA muscles. This is an indication of a change in the phenotype of TA muscles in *Gars*$^{C201R/+}$ mice, since increased staining for SDH shows the increased oxidative capacity of these muscle fibres. In addition, *Gars*$^{C201R/+}$ TA muscle fibres appeared larger than those of wild-type littermate controls. We therefore assessed the cross-sectional area (CSA) of TA muscle fibres in SDH-stained sections of *Gars*$^{C201R/+}$ mice ($n$=3) and wild-type littermates ($n$=3). In *Gars*$^{C201R/+}$ mice, the average CSA of TA muscle fibres is 3130±28 μm$^2$ compared with only 2292±14 μm$^2$ in controls (Fig. 4E). Thus, there is a significant increase in the CSA of TA muscle fibres in *Gars*$^{C201R/+}$ mice compared with in controls ($P$<0.001). This hypertrophy of TA muscle fibres in *Gars*$^{C201R/+}$ mice is accompanied by a significant loss of muscle fibres so that, in *Gars*$^{C201R/+}$ mice, the average number of muscle fibres per muscle section is only 1537±161 compared with 2694±122 in controls (Fig. 4F). Morphometric analysis of the size of muscle fibres reveals that the TA muscles in *Gars*$^{C201R/+}$ mice contain fewer small muscle fibres, as shown in the frequency distribution histogram in Fig. 4G, and a greater proportion of larger fibres than in the TA muscles of wild-type littermates. These results are consistent with denervation atrophy, leading to a decrease in fibre number, and compensatory hypertrophy of the remaining fibres.

The weight and histochemical properties of EDL muscles were also assessed. Although the EDL muscles in *Gars*$^{C201R/+}$ mice weighed less than those in littermate controls (8.58±0.27 grams versus 7.79±0.29 grams, respectively), this reduction in muscle weight was not significant. Histochemical analysis of the oxidative capacity of EDL muscle fibres revealed that the EDL of *Gars*$^{C201R/+}$ mice had a characteristic mosaic pattern of SDH staining. The majority of muscle fibres in *Gars*$^{C201R/+}$ mice stained lightly for SDH, indicating that, similar to the EDL muscle fibres in wild-type littermates, these fibres have a low oxidative capacity (data not shown), consistent with little or no denervation in the EDL.

We also measured the CSA of EDL muscle fibres in SDH-stained sections of EDL from *Gars*$^{C201R/+}$ and wild-type littermates. As observed in the TA, the EDL muscle fibres from the *Gars*$^{C201R/+}$ mice were significantly larger than EDL muscle fibres in wild-type littermates (supplementary material Fig. S4G). Furthermore, there were fewer muscle fibres in the EDL muscle sections of *Gars*$^{C201R/+}$ mice compared with controls (supplementary material Fig. S4H) and, as shown in the size frequency distribution histogram, the fibres that survive are larger than those in control mice (supplementary material Fig. S4J). This is consistent with some denervation, but at the level of individual terminals rather than whole motor units.

To test whether the observed reduction in TA muscle force and loss of muscle fibres in the *Gars*$^{C201R/+}$ TA and EDL were the result of motor neuron degeneration, the number of Nissl-stained motor neurons present in the lumbar spinal cords was assessed. We observed no motor neuron loss in the mutant mice, despite the reduction in TA muscle force and the loss of TA and EDL muscle fibres in these mice at the same age (see supplementary material Fig. S4I). This is consistent with other *Gars* alleles in mice, in which the pathology was in the distal axon and not evident in the spinal cord or ventral roots.

The differential severity in the phenotype of the EDL versus the TA is reflected in the innervation of the neuromuscular junctions (NMJs). In wild-type mice, the EDL and TA both have typical NMJ morphology, with a complex pretzel-shaped appearance and the nerve terminal directly overlying the acetylcholine receptors (AChRs) in the muscle membrane (Fig. 5A,B). In the *Gars*$^{C201R/+}$ mice, the NMJs found on the EDL were, in some cases, fairly normal and, in other cases, much smaller with a much less complex geometry (Fig. 5C,D). In the TA, some NMJs had relatively normal morphology, although regions of the receptor field were sometimes unoccupied by the nerve terminal, and portions of the terminal arbor appeared atrophied (Fig. 5E, blue arrow). Instances of clear denervation were also observed, with some AChR patches completely lacking presynaptic input (Fig. 5E, red arrow). The frequency of such defects was significantly higher in the *Gars*$^{C201R/+}$ TA, with 6.2±3.2% of the NMJs showing marked partial innervation and 3.1±1.2% showing complete denervation compared with 1.6±1.1% and 0.3±0.5%, respectively, in the *Gars*$^{C201R/+}$ EDL ($P$=0.08 and $P$=0.03, respectively, $t$-test; *Gars*$^{C201R/+}$ EDL values were not significantly different from those in control mice). This denervation was muscle specific and an overall reduction in the number of motor axons was not seen in large, primarily motor nerves such as the motor branch of the femoral nerve, which innervates the quadriceps. Control mice had 558±38 myelinated axons in this nerve, whereas *Gars*$^{C201R/+}$ mice had 559±29 ($n$=3 mice per genotype, all mice were 5 months of age).

### Assessment of sensory physiology and histopathology

To assess the properties of peripheral sensory neurons, we studied the purely sensory saphenous nerve in five *Gars*$^{C201R/+}$ mice and three wild-type littermates on the C57BL/6 background. There was no significant difference ($P$>0.3, $t$-tests) in the mean number of myelinated axons (476±15 in *Gars*$^{C201R/+}$ mice; 449±31 in wild-type mice), with no sign of degenerating or demyelinated axons (Fig. 6A,B). However, quantification of axon diameters revealed a significant shift in the axon calibre towards a smaller diameter in the saphenous nerve of *Gars*$^{C201R/+}$ mice compared with wild-type littermate controls (Fig. 6C). Although there were 83±7 axons with

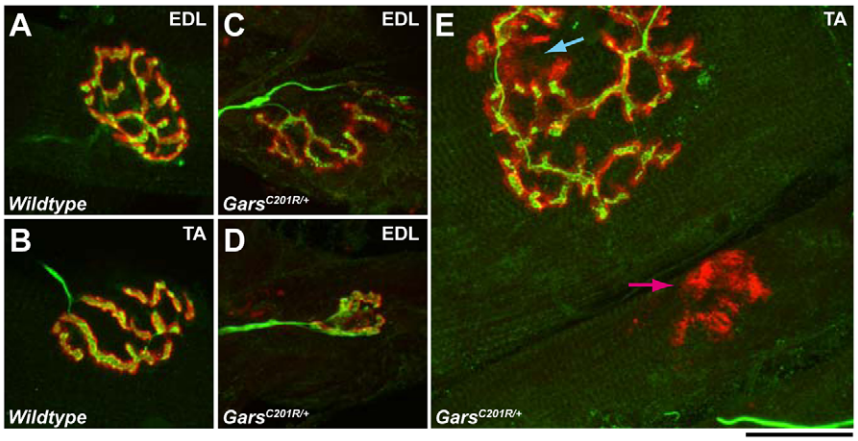


**Fig. 5. NMJ morphology and nerve occupancy.** (A,B) NMJs in the EDL and TA of wild-type mice show typical morphologies. In the *Gars*$^{C201R/+}$ mice, NMJs in the EDL have variable geometries with some being relatively normal (C), whereas others were very small and much less elaborate (D). (E) In the TA, regions of partial innervation were observed (a subtle example is indicated by the blue arrow) and portions of the terminal arbor appear atrophied. Examples of clear denervation were also observed (red arrow). Bar, 7 µm.

a calibre of greater than 3.5 µm in the wild-type mice, this number was reduced profoundly to 13±6 in *Gars*$^{C201R/+}$ nerves ($P$<0.001, $t$-test). Analysis of the hairy skin of the medial dorsum of the hindfoot, corresponding to the innervations territory of the saphenous nerve, and the glabrous skin, which is innervated by branches of the tibial nerve, showed a normal dense plexus of axons in the subepidermis and epidermis in both genotypes of mice (Fig. 6D,E). As epidermal nerve fibre density is derived exclusively from unmyelinated (C-) fibres, there is, therefore, no evidence for a loss of unmyelinated sensory neurons.

### Sensory nerve pathology

There were significant differences in the conduction velocity and amplitude of the Aβ-fibre sensory nerve compound action potential (SNAP) in *Gars*$^{C201R/+}$ mice compared with wild-type littermates, but there were no significant changes for unmyelinated (C-) fibres (Fig. 7). Corresponding to the change in axon calibre of myelinated fibres of the *Gars*$^{C201R/+}$ saphenous nerve, the mean conduction velocity of the Aβ-fibre SNAP was 33.4±0.6 milliseconds in wild-type controls ($n$=8) compared with 23.4±0.8 milliseconds in mutant mice ($n$=7) ($P$<0.001). There was also a small, but significant, drop in the amplitude of the Aβ-fibre SNAP (wild-type, 1.7±0.2 mV; *Gars*$^{C201R/+}$, 1.2±0.2 mV; $P$<0.05) and a trend for a reduced conduction velocity of the C-volley in mutant animals (wild-type, 0.98±0.04 ms; *Gars*$^{C201R/+}$, 0.84±0.06 ms; $P$=0.057). In agreement with a normal subepidermal and epidermal nerve fibre morphology, there was no significant difference in the amplitude of the C-fibre SNAP (wild-type, 312±60 µV; *Gars*$^{C201R/+}$, 474±123 µV; $P$>0.2).

We used nerve excitability testing to determine the strength-duration time constant, the recovery cycle, the threshold electrotonus and the current-threshold relationship in four wild-type mice and six *Gars*$^{C201R/+}$ mice. There were clear differences in the onset and magnitude of the superexcitability and the relative refractory period (RRP) (Fig. 7C), but not in the recovery cycle (Fig. 7D) or the other parameters tested (supplementary material Fig. S5). For a period of approximately 200 milliseconds after an action potential, there are profound changes in the excitability of myelinated axons that manifest as refractoriness, superexcitability and late subexcitability, which reflect nodal and paranodal membrane properties. The balance of transient sodium and fast potassium conductances influences superexcitability. It reflects the net charge that is transferred to the internode (Bostock, 2004) and is best studied following the recovery from a single conditioning stimulus. By contrast, late subexcitability is controlled by slow nodal potassium conductances (mainly by the

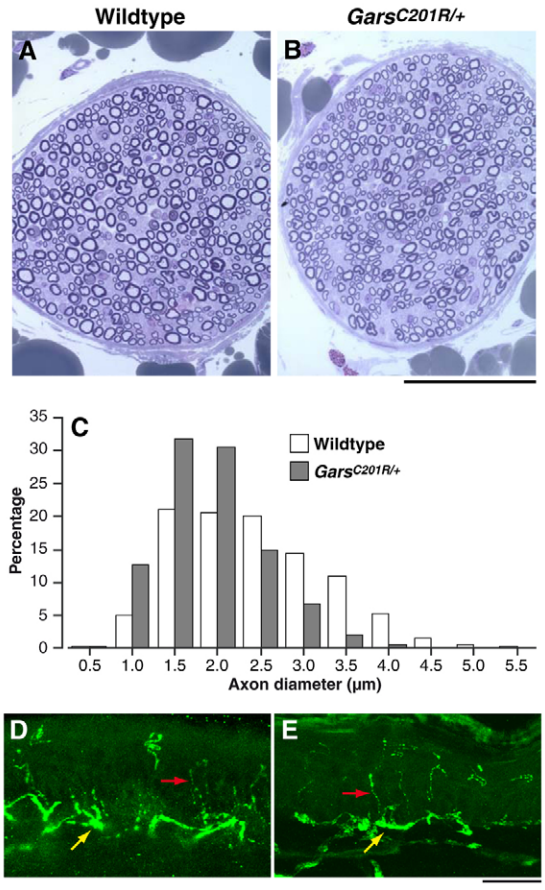


**Fig. 6. Light microscopy of Toluidine Blue-stained, semi-thin resin section of the saphenous nerve from 3-month-old wild-type littermate control (A) and *Gars*$^{C201R/+}$ mutant mice (B) on the C57BL/6 background.** There is no axonal loss, axon degeneration or demyelination, but quantification of axon diameters (C) reveals a shift towards a smaller diameter in the *Gars*$^{C201R/+}$ nerve. (D,E) Confocal fluorescent images of the subepidermal (yellow arrows) and epidermal (red arrows) axons innervating the glabrous skin of wild-type littermate control (D) and *Gars*$^{C201R/+}$ mutant (E) mice. Bars, 70 µm (A,B); 25 µm (D,E).

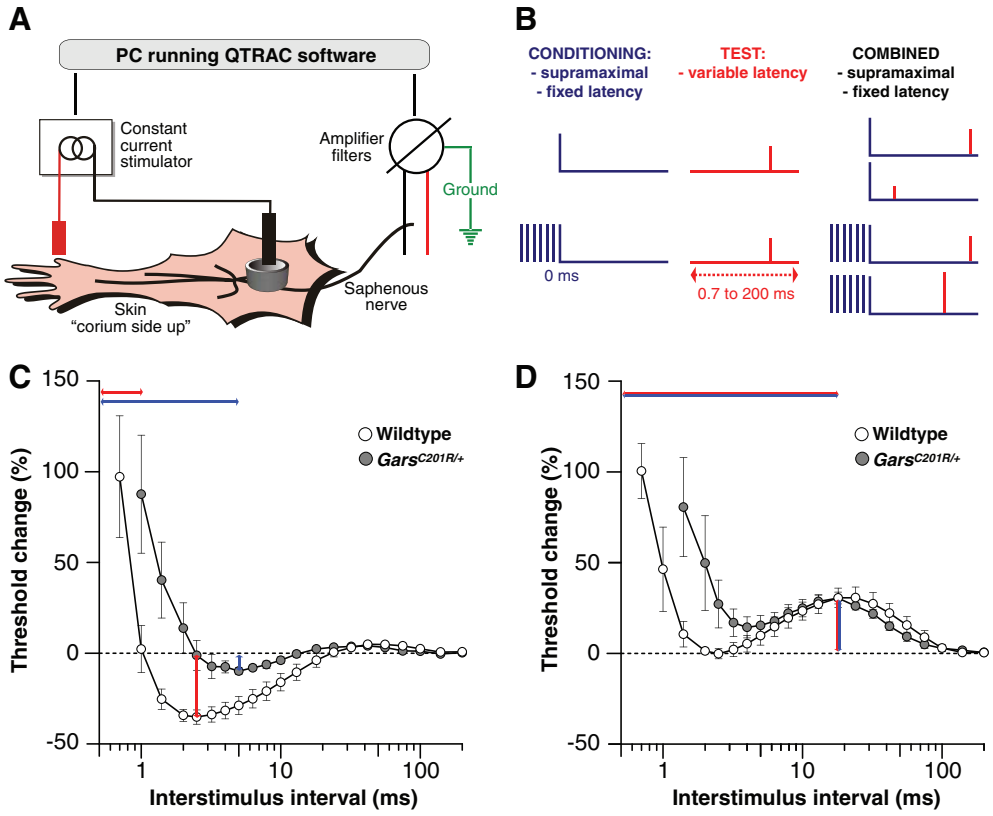


**Fig. 7. Testing conduction velocity and amplitude.** (A) Schematic representation of the setup for nerve excitability testing of the saphenous nerve. (B) Stimulus paradigm for recording the recovery cycle. A single supramaximal conditioning stimulus or a train of seven conditioning stimuli is followed by the test stimulus at a variable latency of 0.7 to 200 milliseconds. (C) In animals carrying the *Gars*$^{C201R}$ mutation, the magnitude of the superexcitability is lower and later in the recovery cycle, and the relative refractory period is longer compared with in wild-type controls. Using a single conditioning stimulus, superexcitability is defined as the decrease of the threshold below the line of neutrality (0 on the ordinate). The magnitude of the maximal threshold reduction is marked for wild-type (red arrow) and *Gars*$^{C201R/+}$ (blue arrow) by vertical arrows. The relative refractory period is defined as the time between zero and the point at which the excitability threshold crosses the line of neutrality. The horizontal arrows show this time period: wild-type (red arrow) and *Gars*$^{C201R/+}$ (blue arrow). (D) The magnitude (vertical arrows) and peak time (horizontal arrows) of the late subexcitability is not significantly different.

M-current Kv7/KCNQ) (Schwarz et al., 2006) and is best seen following application of a conditioning train of action potentials. Corresponding to the delay of conduction velocity, there was a change in the peak of the superexcitability (expressed as a reduction of the threshold) from 2.48±0.31 milliseconds in wild-type mice to 4.82±0.80 milliseconds in mutants ($P$=0.058), and there was a prolongation of the relative refractory period from 1.0±0.1 milliseconds in wild-type controls to 2.2±0.2 milliseconds in mutant nerves. Furthermore, there was a highly significant reduction in the amplitude of the superexcitability from –36±3.5% to –13±2.5% ($P$<0.001).

### Central nervous system (CNS) histopathology of homozygous *Gars*$^{C201R/C201R}$ mice

In 15-day-old *Gars*$^{C201R/C201R}$ mice, we saw potentially abnormal phenotypes in motor areas of the cortex; the dorsal column of the spinal cord; the dorsal root; and the trigeminal ganglia, when compared with heterozygous and wild-type controls (supplementary material Fig. S3B,C); however, sample sizes were small. In the motor cortex, the cell numbers in layer III were reduced [wild-type cell count, 117±13 cells per unit ($n$=2); homozygote cell count, 74±12 cells per unit ($n$=3)]; this was not statistically significant ($P$=0.09), which could be because of the low numbers of mice sampled (supplementary material Fig. S3B). Sensory cortex cell counts were similar between all three genotypes (data not shown).

The mean average CSA of the thoracic dorsal column of homozygotes appeared to be smaller than that of wild-type controls, which would correlate with the small axon calibre found in the dorsal roots of heterozygous animals (supplementary material Fig. S3C); but, again, sample sizes were small.

## DISCUSSION

We identified the Gars$^{C201R}$ founder mice in a phenotype-driven screen that analysed a large set of ENU-mutagenised mice for novel motor mutants. Positional cloning, using grip strength to score for affected animals, led to the identification of a non-conservative cysteine to arginine change in a highly conserved residue in the GARS catalytic domain (Cader et al., 2007; Xie et al., 2007). The effect on grip strength varied with genetic background, in accordance with the variations in presentation seen in humans (Antonellis et al., 2003; Dubourg et al., 2006; Sivakumar et al., 2005); the Gars$^{Nmf249}$ mouse phenotype also varied depending on genetic background (Seburn et al., 2006). Determining the genetic factors that modulate *GARS* mutations may give us intervention points for therapy, and the Gars$^{C201R}$ mouse could be an excellent model in which to find such modifying loci. Intriguingly, a recent paper (Mozhui et al., 2008) has defined a region (*Qrr*) on distal mouse chromosome 1 that modulates the gene expression of more than half of all aminoacyl-tRNA synthetases in CNS tissues, and the effect on *Gars* is particularly strong – the C57BL/6 trans-quantitative trait loci (QTL) allele of *Qrr* has a positive additive effect and consistently increases *Gars* gene expression by 10-30%.

Human *GARS* mutations cause strikingly selective atrophy, weakness and corresponding abnormal neurophysiological profiles of the thenar musculature, with sparing of the adjacent muscles that are innervated by the same segment (for example, the hypothenar musculature). In our studies, the overall picture of the

heterozygous mice is of clear histopathological and electrophysiological deficits in the sensory system, together with deficits in the function of some muscles that are consistent with neurological changes of the motor system; however, there were no clear deficits in motor neurons at the ages studied. Thus, a detailed longitudinal assessment of the motor system of these mice needs to be undertaken. We found that there was a preferential involvement of muscles, such that the large TA muscles were more affected than EDL muscles. However, both muscles show a significant loss of muscle fibres, accompanied by hypertrophy of those muscle fibres that survive. In humans, affected individuals generally have normal sensory, and slightly reduced motor (when there is substantial axonal loss), nerve conduction velocities, suggesting a primary axonal pathology (Del Bo et al., 2006; Sivakumar et al., 2005). In contrast to humans, a reduction of sensory ($Gars^{C201R/+}$) and motor conduction velocity ($Gars^{Nmf249/+}$) (Seburn et al., 2006) is found in the Gars mouse models. As histological studies have failed to find signs of primary demyelination in $Gars^{C201R/+}$ mice, but have found a reduction of axon calibre, the reduction in conduction velocity is best explained by the dropout of the largest and fastest conducting axons. The changes in the recovery cycle are consistent with this interpretation.

The muscle specificity of the phenotype is consistent with human CMT2D. The defects seen in NMJ occupancy are much milder than those observed previously in $Gars^{Nmf249/+}$ mice and, when combined with the lack of axon loss even in distal nerves such as the femoral motor branch, may indicate that the degeneration in $Gars^{C201R/+}$ mice occurs at the level of individual motor neuron terminals, and not at the level of motor axons (motor units). The percentages stated may be underestimates owing to variability in antibody staining, the subtlety of the partial innervation, and the fact that denervated muscle fibres may have atrophied in 5-month-old mice, preventing their inclusion in this analysis. As with the NMJ innervation, the relative preservation of axon diameter and myelinated axon number, even in more distal nerves, also indicates that the $Gars^{C201R}$ allele is much milder than the $Gars^{Nmf249}$ allele. In this regard, the $Gars^{C201R/+}$ mouse may present a more accurate model of human CMT2D. An intriguing question to be addressed in this mouse model is, how much of the phenotype occurs as a developmental defect and how much arises later from degeneration? We note that we see relatively little loss of function over time in the grip strength analysis and, thus, at least a component of the phenotype probably arises early in the life of the animal; although, only a detailed longitudinal study of motor, sensory and muscle phenotypes could determine if the mutation results in developmental and/or degenerative changes. We note that we have studied the $Gars^{C201R}$ mutation on two inbred mouse backgrounds that clearly give rise to different phenotypes. The results of *GARS* mutations in humans are highly variable, ranging from asymptomatic individuals at over 40 years of age to severe infantile disease (Dubourg et al., 2006; James et al., 2006); thus, both human and mouse manifest variable severity arising from different alleles and genetic backgrounds.

We produced homozygotes that, for the first time, show the effects of having two copies of a *Gars* point mutation; the mild phenotype found in heterozygous animals becomes a pre-weaning lethal disorder, resulting in what appear to be extensive deficits in the brain and spinal cord in homozygotes. We found no differences in protein levels (by western hybridisation) between adult heterozygous and wild-type mice at 3 months of age, but a significant increase in protein levels in heterozygotes and homozygotes at 15 days of age compared with in wild-types. This may indicate that the level of GARS is more crucial during development than in adult mice; clearly the developmental profile of this enzyme warrants further investigation. We note that no difference in GARS protein levels was found between lymphoblastoid cell lines from a human $GARS^{G240R/+}$ heterozygous patient and a wild-type individual (Antonellis et al., 2006); this is similar to our findings for adult $Gars^{C201R/+}$ heterozygous mice compared with wild-type mice.

We found a 60% reduction in enzyme activity in the dissected brain homogenate of homozygous mice (15 days of age), but no significant difference between wild-type and heterozygous animals at 15 days or 3 months of age; however, there was a trend towards reduced enzyme activity in the heterozygotes compared with the wild-type mice. The rise in protein levels in homozygous and heterozygous animals at 15 days of age may be compensation for reduced enzyme activity, possibly during a crucial developmental window. The $GARS^{C201R}$ mutation impairs enzyme function but our data also suggest that wild-type–$GARS^{C201R}$ heterodimers retain more activity compared with mutant homodimers. Further work is required to determine the extent of heterodimer formation and the effects of $GARS^{C201R}$ on heterodimeric and homodimeric enzyme activity (Nangle et al., 2007). The non-viability of compound heterozygote mice carrying both the gene trap loss-of-function $Gars^{XM256}$ allele and either the $Gars^{C201R}$ allele or the $Gars^{Nmf249}$ allele with fully retained activity (both compound heterozygotes were embryonic lethal), suggest that there may be functional interactions between wild-type and mutant proteins) (Seburn et al., 2006).

A dominant negative activity or partial loss of function of the $Gars^{C201R}$ allele is possible; this is supported by the increase in phenotypic severity with increased dosage in either homozygotes or in the absence of wild-type homodimers. However, a gain-of-function mechanism cannot be dismissed for heterozygous mice, since the overall activity of GARS is preserved in tissues. Structural studies have revealed that the $GARS^{Nmf249}$ mutation and a majority of the reported human GARS mutations affect the dimer interface, sometimes through distant interactions, resulting in increases and decreases in dimerisation; however, it remains unclear how this relates to disease pathogenesis (Cader et al., 2007; Xie et al., 2007). Chihara and colleagues found that Drosophila models, which had previously been used to describe human GARS mutants, have loss-of-function properties (Cader et al., 2007; Chihara et al., 2007); furthermore, studies in yeast have also demonstrated loss-of-function effects for some GARS mutants, but no dominant negative effects (Antonellis et al., 2006). However, studies of aminoacylation activity do not support a straightforward loss-of-function mechanism since there is no correlation between the CMT phenotype and enzyme activity (Nangle et al., 2006). Nevertheless, mutant GARS proteins have aberrant distributions within cells (Antonellis et al., 2006) and reduced expression in the neurite periphery (Nangle et al., 2006).

Drosophila with mutations in the *gars*, tryptophanyl-tRNA synthetase (*wars*) or glutaminyl-tRNA synthetase (*qars*) genes show that cytosolic tRNA synthetase activities are needed for axonal

maintenance during development, but that mitochondrial tRNA synthetase activities have a greater role in maintaining dendrites in adults (Chihara et al., 2007). The Drosophila mutations are loss-of-function alleles and, unlike the mouse and human mutations, all were recessive. Mutations in other aminoacyl-tRNA synthetases are now starting to be described and may help our understanding of how aberrations in these ubiquitous housekeeping enzymes result in specific pathologies within the nervous system (Edvardson et al., 2007; Scheper et al., 2007). Mutations in the human tyrosyl-tRNA synthetase (*YARS*) gene were found to cause dominant intermediate CMT type C, possibly owing to a partial loss of enzyme activity giving rise to pathology at the neuron endings (Jordanova et al., 2006). In the mouse, a recessive mutation in the alanyl-tRNA synthetase (*Aars*) gene causes cerebellar Purkinje cell loss and ataxia, probably because of a partial loss of the editing function of the enzyme, leading to a low level of amino acid misincorporation and, hence, protein misfolding and neurodegeneration (Lee et al., 2006). In cultured human cells, a mutant form of the valyl-tRNA synthtase (VARS) protein with defective editing ability caused cell death (Nangle et al., 2006).

All of the GARS point mutations described so far in mice and humans are dominant, implying that the phenotypes arise from either a dominant gain-of-function mutation or haploinsufficiency. Drosophila and mouse studies suggest that, depending on the individual mutation, both of these causes are possible (Chihara et al., 2007; Seburn et al., 2006). From our studies, either mechanism is possible, and we also suggest another scenario in which the phenotype could arise from a loss-of-function mutation (such as loss of enzyme activity, as seen in the homozygous $Gars^{C201R/C201R}$ mice) and a gain-of-function mutation, as suggested in the $Gars^{Nmf249}$ model (Seburn et al., 2006); different pathological mechanisms may be crucial at different time points in both heterozygotes and homozygotes, that is, there could be a gain of a new function leading to a toxic effect, combined with a loss of function.

In terms of the effects on GARS function, loss of enzyme activity might directly affect local translation, which is essential for axon guidance, synaptic plasticity, cell migration, cell polarity, and other areas of development and maintenance of the nervous system (Giuditta et al., 2002; Jordanova et al., 2006; Lin and Holt, 2007; Nangle et al., 2007; Park et al., 2008). Alternatively, it has been postulated that GARS mutations could result in phenotypes either because of a defect in translating proteins that contain glycine or because the mutations affect a glycine-rich subset of proteins in neurons (Antonellis et al., 2003); in fact, a set of cytoskeleton-associated proteins (CAPs) and motor proteins involved in axonal transport contain a glycine-rich CAP-Gly motif that binds to microtubules during long-range transport (Li et al., 2002; Sivakumar et al., 2005; Weisbrich et al., 2007). We carried out a search for this motif in the human genome (by looking for protein sequences containing the motif) and found that fewer than ten proteins contain it, suggesting that aberrations in the translation of this CAP-Gly motif are unlikely to be causative of the phenotypes because relatively few proteins carry it; however, we do not have information on how crucial the individual levels of each of these ten proteins are within neurons. Intriguingly, mutations in the CAP-Gly motif in dynactin p150 and in tubulin-specific chaperone B are known to cause peripheral motor neuron degeneration in humans and mice (Li et al., 2002; Martin et al., 2002; Puls et al., 2003; Sivakumar et al., 2005). Furthermore, we note that TAR DNA binding protein (TDP-43), which causes cases of ALS, contains a glycine-rich domain (Banks et al., 2008).

However, although aminoacylation is the only known function for GARS, a wide range of non-canonical functions has been shown for other aminoacyl-tRNA synthetases, including an involvement in splicing, apoptosis, transcription, protein folding, and trafficking (Park et al., 2005; Park et al., 2008; Jia et al., 2008; Ribas de Pouplana and Geslain, 2008). Thus, it is possible that heterozygous and/or homozygous phenotypes do not arise from defects in translation, but arise because of aberrations in other, unknown, functions of GARS.

## METHODS

Wherever possible, all of the methods described below were undertaken blind to mouse genotype, which was decoded after the results were collected.

### Mice

The $Gars^{C201R}$ mutation arose in an ENU mutagenesis experiment at the MRC Mammalian Genetics Unit, Harwell, UK (Nolan et al., 2000). A G0 mutagenised BALB/cAnN male produced two male siblings, MUTN/610.6c and MUTN/610.6d and sperm from these animals was used for in vitro fertilisation of C3H/HeH females in the stock matings GENA201 and GENA202, respectively. As ENU works on spermatagonial stem cells, one treated mouse may produce multiple progeny derived from the same mutation in the same stem cell. The resulting N2 progeny were backcrossed to C3H/HeH or C57BL/6J mice. Intercrosses to produce homozygous animals were carried out as described in the text. All animal studies were carried out under the guidance issued by the MRC on 'Responsibility in the use of animals for medical research' (1993) and under licence from the UK Home Office.

### Grip strength testing

The grip strength test assessed neuromuscular function by measuring, with an electronic digital force gauge, the peak amount of force an animal applied in grasping a 10×8 centimetre wire grid attached to a pull bar (Bioseb Instruments). The mouse was placed on the flat wire grid connected to the force gauge and held on with front and hindpaws. The mouse was held by the base of the tail and was gently pulled away from the grid until it released its grip, at which point the peak tension on the pull bar was recorded. The mean of five measurements was determined for each mouse on each day of testing. Further details of the standard operating procedure for grip strength that we followed can be found at the Eumorphia site http://empress.har.mrc.ac.uk/browser/.

Mice were scored as affected if their mean measure differed by more than three standard deviations from the mean score for a cohort of age- and sex-matched wild-type controls that had been bred onto the same genetic background (C3H/HeH or C57BL/6J) at the same generation.

### MoRaG performance

We tested nine male $Gars^{C201R/+}$ mice and ten male wild-type littermate controls in two MoRaG test sessions over two consecutive days. All mice were bred onto the C3H/HeH genetic

background. The MoRaG test is a phenotyping assay that was created to characterize fine motor behaviours in the mouse (Tucci et al., 2007). The apparatus consists of a Plexiglas chamber with a feeding platform on the outside front wall. Mice are primed to perform in the task by restricting access to food for up to 16 hours before the task. Prior to commencing the task, mice were placed in the apparatus for a 5-minute acclimatisation period. Small food pellets were then placed on the feeding platform at a distance of approximately 1.5 centimetres. As the opening is not large enough for the mouse to collect the food pellet using its mouth, the mouse learns to use one or both forelimbs. Each trial began when the pellet was delivered to the feeding platform and ended when the mouse collected it. The intertrial interval varied from between 10 and 20 seconds. Performance in the task was assessed using semiquantitative and quantitative parameters [see Tucci et al. (Tucci et al., 2007) for a complete list of the parameters]. Semiquantitative parameters were selected from a wide range of abnormalities that may affect neurological, neuromuscular and behavioural function (e.g. tremor, speed of movement, body and shoulder position, posture). Three quantitative behaviours were also recorded: (1) reaction times to reach the food pellets; (2) reaching accuracy; (3) grasping accuracy. The LFR is an index of flexibility of the mouse in changing from a default motor response (e.g. nose poking) to a novel motor pattern (limb movement). Each session consisted of 30 consecutive trials lasting approximately 15-20 minutes in total. Reaction times from the first ten trials were recorded. The MoRaG data were analysed using the SPSS statistical package (SPSS, Chicago, IL). Reaction times and LFRs within the session were analysed by an analysis of variance (ANOVA) test.

### Genetic mapping

To map the GENA201 and GENA202 mutations, N3 mice from the C3H backcross were assessed for grip strength and scored as affected by the criterion above. A whole genome scan using 72 SNPs that were polymorphic between the C3H and BALB/c strains and that were spaced every 20-40 Mbs across the 19 autosomes was performed on 13 affected GENA201 and 13 affected GENA202 heterozygotes. For GENA201 mice, linkage was found to chromosome 6 at between 22 Mb and 114 Mb, and for GENA202 mice, linkage was found between 22 Mb and 84 Mb, as stated in the text. The critical region was narrowed by using a higher density set of polymorphic microsatellite markers [D6Mit273 (46 Mb), D6Mit183 (53 Mb), D6Mit384 (55 Mb), D6Mit186 (73 Mb), D6Mit188 (75 Mb)] to haplotype map 61 affected animals, from both the C3H (N3) and C57BL/6 (N2) background, for GENA201 and 29 affected mice, from both the C3H (N3) and C57BL/6 (N2) background, for GENA202. Results from this haplotype analysis showed that the mutation must lie within a BALB/c-derived critical region defined by SNPs and a microsatellite at 53.8 Mb (refSNP ID: rs3023070) and 73 Mb (D6Mit186) for GENA201 and at 53.8 Mb (refSNP ID: rs3023070) and 58.5 Mb (refSNP ID: rs13478778) for GENA202 mice (all mapping positions are based on the mouse genome sequence in NCBI Build 36, http://www.ncbi.nlm.nih.gov). The GENA202 critical region between 53.8 and 58.5 Mb contained 63 genes (NCBI Build 36), including *Creb5*, *Chn2* and *Neurod6*, which are known to be involved in neuronal function and/or have neuronal phenotypes when mutated. However, other than *Gars*, none of the genes in the critical region were likely to give rise to the GENA201 or GENA202 phenotypes because of either the expression pattern or the existing functional data. The complete *Gars* gene (all 17 exons and associated splice sites) was sequenced in GENA201 and GENA202 mice, and the same mutation was found in exon 5, conferring a non-conservative amino acid change on the protein in both cohorts of affected mice.

### Sequence analysis and routine genotyping

DNA was extracted from mouse tail tips using a genomic DNA isolation kit (Promega UK Ltd). A primer pair per exon was used for PCR amplification of the 17 exons of the *Gars* gene in wild-type, heterozygous and homozygous mutant DNA from GENA201 and GENA202 mice. DNA sequences were resolved on an automated MegaBACE 1000 DNA analysis system (Amersham Pharmacia) and the base pair change in exon 5 was found. This mutation introduces a restriction site for the enzymes *Hae*II and *Hha*I, allowing a protocol to be designed for routine genotyping by PCR followed by RFLP analysis. Routine genotyping: PCR primers (forward: 5′-CACGTGCTTGCTCTAGCAAGA-3′; reverse: 5′-GTCTACCACTGAACACAGTCC-3′) that are complementary to regions within intron 4 and intron 5, respectively, and thus span exon 5 of the *Gars* gene, were used to amplify a 420 bp product. This amplicon was digested with *Hha*I to give fragments of 420 bp (there is no restriction site in the *Gars* loci of wild-type BALB/c, C3H and C57BL/6 mice) and of 250 bp and 170 bp ($Gars^{201R}$ mutant gene).

### Western hybridisation and enzyme activity

Mice from the C3H backcross were from generation N5 or N6 and mice from the C57BL/6 backcross were from generation N3 or N4. Mice were killed according to UK Home Office regulations and brains were removed, dissected and the motor/sensory cortex-containing region was flash frozen in liquid nitrogen. 10 mg of brain per ml of buffer [50 mM Tris pH 7.5, 25 mM KCl, 1% NP40, 10% glycerol, 1 mM DTT, 10 μl protease inhibitor cocktail (Sigma) per ml] was homogenised using a plastic mortar and then centrifuged in a microcentrifuge for 20 minutes at 12,000 rpm at 4°C. Supernatant was aliquoted into 100 μl samples and stored at –80°C until used. The protein concentration of a supernatant sample from each brain was determined using a bicinchoninic acid assay (Pierce).

Homogenates were electrophoresed on polyacrylamide-Tris gels (16% or 4-20% gradient) and then transferred onto a polyvinylidene difluoride (PVDF) membrane (ImmobilonP). Membranes were washed for 1 hour in blocking solution (5% w/v skimmed milk powder, 0.05% Tween 20 in PBS), before addition of the anti-GARS antibody (a gift from Kevin Talbot) in blocking solution at 4°C overnight. The primary antibody was detected using AP-conjugated anti-rabbit IgG (Sigma) and the results visualised using CPD-Star (Roche). The blots were then stripped and reprobed using an antibody against β-actin (Sigma A5441). Autoradiographs were quantified using Imagemaster 1D software (Amersham Pharmacia Biotech) and the GARS levels normalised for β-actin levels.

The same dissected brain protein homogenates were used to measure GARS enzyme activity (Dignam and Dignam, 1984). One 100 μl sample was assayed from each brain for GARS activity: the sample was split into three aliquots of 20 μl each and each aliquot was assayed for GARS activity. To measure GARS activity, 60 μl of reaction mix [10 μM glycine, 50 mM Tris pH 7.5, 25 mM KCl, 2 mM

DTT, 10 mM magnesium acetate, 5 mM ATP, 2 µl RNAse inhibitor (Ambion), 1 µM $^{3}$H-glycine (740 GBq/mMol, Amersham Biosciences)] was added to each 20 µl brain supernatant sample and the mix was incubated at 37°C for 20 minutes. 80 µM of tRNA-bovine liver (Sigma) was added and the reaction was incubated for a further 5 minutes at 37°C. The reaction mix was spotted on 3 MM Whatman filter paper and washed once in 10% trichloroacetic acid (TCA) for 15 minutes, three times in 2.5% TCA for 15 minutes and once, for a further 15 minutes, in 100% ethanol. The filter was then air-dried and 5 ml of scintillation fluid (Ultima Gold, PerkinElmer) was added. The samples were counted in a scintillation counter, which reported the number of photons detected as counts per minute (cpm). Each reaction mix was spotted and counted three times. The difference between cpm and disintegration per minute (dpm) is the efficiency of the counter in detecting the release of β-particles. To obtain dpm, the mean of each sample count was divided by the efficiency of the assay: dpms were converted to disintegration per second and then divided by the specific activity of the radioactive glycine to obtain pmoles. The result was normalised using the protein concentration to obtain pmoles per mg of protein per minute. For the negative control, the reactions were processed as above, but no tRNA was added. For the positive control, tryptophan activity was measured ($^{3}$H-tryptophan, 740 GBq/mMol, Amersham Biosciences) to check that other aminoacyl transferases showed normal activity in the brain homogenate. On the C3H background, tryptophan mean activity in 3-month-old wild-type mice ($n$=5) was 52.6±5.4 pmole/mg/min compared with 59.1±1.3 pmole/mg/min for $Gars^{C201R/+}$ littermates, and for 15-day-old C3H littermates, the activity was 48.6±2.5 pmole/mg/min for wild-type mice ($n$=3), 43.0±6.6 pmole/mg/min for $Gars^{C201R/+}$ mice ($n$=3) and 45.7±4.2 pmole/mg/min for $Gars^{C201R/C201R}$ mice ($n$=3).

### General histology

Organs (heart, lung, liver, kidney, adrenal gland, skin, gut and skeletal muscle, including triceps, quadriceps and gastrocnemius muscles) from three wild-type and six $Gars^{C201R/+}$ mice at 17 months of age, and the whole carcass of two wild-type, two $Gars^{C201R/+}$ and three $Gars^{C201R/C201R}$ mice at 15 days of age, were fixed in formalin, embedded in paraffin, cut into sections of 2-5 µm thickness, and stained with haematoxylin and eosin (H&E). All mice were on the C3H background.

### Brain and nerve histopathology and neuron counts

Brain and spinal cord (lumbar, thoracic and cervical levels) paraffin sections were cut from the above group of mice; stained with H&E and Luxol Fast Blue-Cresyl Violet; and immunostained for glial fibrillary acidic protein and choline acetyl transferase. Neurons from a 250×750 µm area (1 unit) of the primary motor cortex were counted and analysed using a Student's two-tailed $t$-test.

Sciatic nerve sections were fixed in a solution of 4% paraformaldehyde (PFA) at room temperature. Specimens were washed, stained with unbuffered aqueous 1% osmium tetroxide (BDH), dehydrated and embedded in araldite epoxy resin (Leica). Semi-thin sections (0.5-1 µm) were cut on an Ultracut E ultra microtome (Leica), stained with 1% Toluidine Blue (BDH), and examined under a Dialux light microscope. Ultra-thin sections (70-100 nm) were collected on copper grids, stained with uranyl acetate and lead citrate (BDH), and examined under a JEOL JEM1230 transmission electron microscope. Neuron cells from a 145×100 µm area of the sciatic nerve cross section were counted and analysed using a Student's two-tailed $t$-test.

For dorsal and ventral spinal root morphometry studies, mice on the C57BL/6 background were transcardially perfused, under terminal pentobarbitone anaesthesia, with a fixative consisting of 3% gluaraldehyde in 0.05 M sodium cacodylate buffer at pH 7.4. Right L4 and L5 dorsal root ganglia with the attached dorsal and ventral roots were dissected, post-fixed in 1% osmium tetroxide (Agar Scientific) and processed into araldite CY212 epoxy resin (Agar Scientific) through graded alcohols and propylene oxide using a standard protocol. Semi-thin sections (0.8 µm) were cut on an Ultracut E ultra microtome (Leica), stained with 1% Toluidine Blue containing 1% borax (BDH), and examined with a Dialux light microscope. The saphenous nerve was immersion fixed for 5 minutes in dead mice, and a piece that was distal to the medial articular nerve was taken, post fixed and processed as described for the spinal roots.

The saphenous nerve (C57BL/6 background) and the L4 and L5 dorsal/ventral roots were photographed at a 40× magnification. The number of myelinated axons and their area was measured using Photoshop CS3 and axon diameter (excluding the myelin sheath) was calculated assuming circularity. The density and total number of myelinated axons were calculated from the images (145×100 µm) and area measurements of the nerve/roots, respectively, using a Leica Quantimet image analyser.

Samples of the hairy skin from the medial dorsum of the foot of the hindlimb and from the glabrous skin of the hindpaw (C57BL/6 background) were fixed in 4% PFA and 50 µm-thick sections were cut on a cryostat. Free-floating sections were immunostained for the panaxonal marker PGP9.5 using a rabbit polyclonal antibody (1:500, Ultraclone, UK) and an anti-rabbit Alexa Fluor 488-conjugated secondary antibody (IgG) (Invitrogen, UK) and visualised on a Leica epifluorescence or a Zeiss 510 LSM confocal microscope.

### Assessment of muscle force and motor unit number

The maximum force of the TA and EDL muscles was assessed in adult female N2 mice at 4 months of age. The animals were anaesthetised (4.5% chloral hydrate solution, 1 ml/100 g body weight, i.p.; Sigma-Aldrich, Poole, UK) and prepared for isometric tension recordings of muscle contraction (Kieran and Greensmith, 2004). The distal tendons of the TA and EDL muscles were exposed, dissected from the surrounding tissue, and cut. The hindlimbs of the animals were then secured rigidly to the table with stainless steel pins and the distal tendons of the TA and EDL muscles were attached to an isometric force transducer (Dynamometer UFI Devices) with silk thread. The sciatic nerve was exposed and sectioned, and all branches were cut except for the deep peroneal nerve that innervates the TA and EDL muscles. The length of the muscles was adjusted for maximum twitch tension. The muscles and nerves were kept moist with saline throughout the recordings and all experiments were carried out at room temperature (23°C). Isometric contractions were elicited by stimulating the nerve to TA and EDL using square-wave pulses with a duration of 0.02 milliseconds, and by supramaximal intensity through platinum electrodes. Tetanic contractions were

elicited by trains of stimuli at a frequency of 40, 80 and 100 Hz. Maximum twitch and tetanic tension, and time to peak and half-relaxation time values were measured using a computer and appropriate software (Scope). The number of motor units in both EDL muscles was assessed by applying stimuli of increasing intensity to the motor nerve, resulting in stepwise increments in twitch tension, owing to the successive recruitment of motor axons. The number of stepwise increments was counted to give an estimate of the number of functional motor units present in each muscle.

### Fatigue test

At the end of the isometric tension recordings, the fatigue pattern of the EDL muscles was assessed by repeatedly stimulating the muscle at 40 Hz for 250 milliseconds every second for 3 minutes, and the contractions were recorded on a pen recorder (Lectromed multitrace 2, UK). EDL is normally a fast fatiguable muscle that fatigues rapidly when stimulated repeatedly. From each fatigue trace, the decrease in tension after 3 minutes of stimulation was measured and a fatigue index (F.I.) was calculated: (initial tetanic tension/tetanic tension after stimulation)/initial tetanic tension.

### Muscle weight, histochemistry and morphometry

At the end of each in vivo physiology experiment, the TA and EDL muscles (C57BL/6 background) were removed, weighed, snap frozen in isopentane cooled in liquid nitrogen and stored at –80°C until processing. Serial cross sections (10 μm) of TA and EDL muscles were cut on a cryostat and stained for SDH activity to determine the oxidative capacity of the muscle fibres, as described previously (Kieran and Greensmith, 2004). TA and EDL muscle sections were examined under a light microscope (Leica DMR) using Leica HC PL Fluotar objectives (10×, 20× and 40× magnification). The total number and CSA of mutant and wild-type muscle fibres were calculated from SDH-stained muscle sections. In addition, the total number of muscle fibres from three sections from the belly of TA and EDL muscles from $Gars^{C201R/+}$ mice ($n$=3) and wild-type littermate control mice ($n$=3) were counted. For each muscle section, the CSA of ~2000 (±87) muscle fibres (approximately 70% of the TA muscle) and ~350 (±51.2) muscle fibres (approximately 50% of the EDL muscle) were calculated by tracing around the fibre perimeters using Leica software. The analysis of CSA of muscle fibres is more accurate in exposing changes in fibre size than measuring other parameters such as muscle fibre diameter (Gorio et al., 1983).

### Motor neuron survival

Following removal of the hindlimb muscles, the mice (C57BL/6 background) were perfused transcardially with 4% PFA in 0.1 M PBS. The lumbar region of the spinal cord was removed, post-fixed in 4% PFA for 6 hours and cryoprotected in 30% sucrose for a minimum of 8 hours. Serial transverse sections (20 μm) were cut using a cryostat and stained with gallocyanin, a Nissl stain. Spinal cord sections were examined under a light microscope (Leica DMR) using Leica HC PL Fluotar objectives (10×, 20× and 40× magnification). The numbers of Nissl-stained motor neurons in the sciatic motor pool of every third section ($n$=60) between the L2 and L5 levels of the spinal cord were counted. Only large (diameter >12 μm) polygonal neurons with a distinguishable nucleus and nucleolus and a clearly identifiable Nissl structure were included in the counts. Images were captured using a Nikon E995 digital camera and the images were downloaded into Adobe Photoshop CS. To optimise image contrast, 'levels adjustment' operations were performed, but no other image manipulations were made.

### Statistical analysis for muscle and motor neuron studies

Statistical significance among the groups was assessed using a Mann-Whitney $U$-test, Student's $t$-test and ANOVA. Significance was set at $P$<0.05.

## TRANSLATIONAL IMPACT

### Clinical issue

Charcot-Marie-Tooth (CMT) diseases are hereditary sensory neuropathies, which affect up to 1 in 2500 individuals. They are characterised by distal muscle weakness and impaired sensation. A related set of peripheral nervous system disorders are the hereditary motor neuronopathies (HMNs), which lead to muscle wasting and death in severe cases. These diseases are difficult to model owing to phenotypic variance and the lethality of known mutations in mice. Recently, mutations in a single gene, encoding the enzyme glycyl-tRNA synthetase (GARS), were found in familial cases of both CMT and severe infantile HMN. GARS function is ubiquitously important for protein translation, where it is necessary to load glycine into proteins, but it is not clear why mutations in the *GARS* gene result in neurological disease. New evidence shows that the activity of GARS and other amino acid transport enzymes is present in nerve terminal ends, away from the cell body where such activities were thought to take place. Furthermore, several recent papers show that mutations in other tRNA synthetases cause neurological effects. However, the purpose of tRNA synthetase in neuron terminals is unknown and it is possible that their undiscovered functions may contribute to neuropathy.

### Results

We describe a new mouse model with a dominant mutation in the *Gars* gene, which displays a spectrum of disorders reminiscent of disease in humans, particularly the CMTs. The mutation has sensory effects, which include the loss of electrical conductance in certain nerves and muscle abnormalities. Although heterozygous mice have a relatively mild phenotype, these animals have defects at the neuromuscular junction. Intriguingly, phenotypes vary depending on the genetic background, concordant with a recent genetic study, which identified that a single regulatory locus controls expression of many of the tRNA synthetases in the mouse. Very few homozygous mice survive to birth and all die within 17 days of birth. Still, this is the first report of successful breeding of homozygous animals with this mutation, and the unique access to material from homozygous animals allows for comparison of enzyme levels and activities between wild-type, heterozygous and homozygous animals. The authors' findings suggest that, in addition to its role in neuropathy, the GARS enzyme may be particularly important during development.

### Implications and future directions

This new mouse model shows many similarities to human mutations in GARS, including phenotype variability, which in this study is influenced by the unique genetic background of two different inbred mouse lines. This indicates that other genes in the genome can modulate the GARS phenotype and that the products of these genes may represent accessible targets for therapeutics. The production of homozygous mice for study will enable the characterisation of the GARS enzyme defects that contribute to human diseases such as CMT and HMN, and the role of this enzyme during development and aging. Furthermore, this model should provide insight into the contribution of other tRNA synthetase defects on nervous system pathology.

doi:10.1242/dmm.003541

### Studies of neuromuscular junctions

Muscles were dissected, fixed by immersion in 2% buffered PFA, and compressed and mildly teased before staining. Staining was performed using a cocktail of anti-neurofilament (2H3), anti-SV2 (Developmental Studies Hybridoma Bank) and Alexa Fluor 594-conjugated alpha-bungarotoxin (Invitrogen/Molecular Probes). Images were collected on a Leica SP5 confocal microscope as serial Z sections and projections are shown.

### Sensory nerve conduction studies

SNAPs of the Aβ- and C-fibres were recorded in the saphenous skin nerve in vitro preparation (C57BL/6 background), as described previously (Koltzenburg et al., 1997; Maurer et al., 2007). The skin of the hindlimb, with the saphenous nerve attached, was removed and mounted corium-side up in an organ bath (Fig. 6A) and superfused with synthetic interstitial fluid (SIF) consisting of (in mM): 108 NaCl, 3.48 KCl, 3.5 $MgSO_4$, 26 $NaHCO_3$, 1.5 $CaCl_2$, 9.6 sodium gluconate, 5.55 glucose, 7.6 sucrose and 10 HEPES, titrated with NaOH to pH 7.4. The temperature of the bath was maintained at 32°C and continually gassed with oxygen. The proximal end of the nerve was desheathed and positioned in a separate recording chamber filled with liquid paraffin. Recordings were obtained in common rejection mode using gold wire electrodes. A self-sealing stainless steel ring was placed on top of the saphenous nerve and the SIF replaced by paraffin oil. The whole nerve was stimulated using non-polarisable Ag/AgCl electrodes, with the cathode positioned in the ring and the anode outside in the organ bath. Compound action potentials were recorded with an isolated custom-made amplifier, using an amplification of 1000-10,000×, and using a 1 Hz high-pass filter and a 1 kHz low-pass filter. The amplitude of the SNAP was measured peak-to-peak, and conduction velocity was determined as the distance between the stimulating and recording electrodes divided by the latency to the beginning of the negative peak of the SNAP. We measured several parameters of nerve excitability including the strength-duration time constant, recovery of excitability after a supramaximal stimuli, and accommodation to conditioning subthreshold polarising stimuli, such as threshold electrotonus or the current-threshold relationship (supplementary material Fig. S5). All values are expressed as mean±s.e.m. and are compared statistically using unpaired *t*-tests.

#### ACKNOWLEDGEMENTS

This work was supported by the Amyotrophic Lateral Sclerosis Association (V.B.-F., L.G., E.M.C.F.); Brain Research Trust (R.C., L.G., E.M.C.F.); European Commission Sixth Framework Programme NEST-2003-1 Adventure Programme12702 (J.v.M., M.K.); Medical Research Council (UK) (V.T., P.M.N.); UK MRC Centre for Neuromuscular Disease (M.A.-Q., S.B., M.K., L.G., E.M.C.F.; G0500288 to E.M.C.F.); Motor Neuron Disease Association (F.A., J.E.M., E.M.C.F.); National Institutes of Health NS054154 (R.W.B.); Robert Packard Center for ALS Research at Johns Hopkins (V.B.-F., L.G., E.M.C.F.); Wellcome Trust (UK) 076700 (G.T.B., E.M.C.F.). We thank Debra Brooker, David Dignam, Eriani Gilbert, Leslie Nangle, Zuzanna Tymowska-Lalanne, James Stevens and Sara Wells for generous support with either mouse or enzyme studies, and Ray Young for graphics. We are also grateful to Christiana Ruhrberg for developmental analysis of heterozygous embryos. Deposited in PMC for immediate release. This article is freely accessible online from the date of publication.

#### COMPETING INTERESTS

The authors declare no competing financial interests.

#### AUTHOR CONTRIBUTIONS

Conceived and designed the experiments: F.A., V.B.-F., H.P.W., G.T.B., V.T., R.W.B., S.B., J.E.M., M.K., L.G., P.M.N. and E.M.C.F. Performed the experiments and analysed the data: F.A., V.B.-F., H.P.W., G.T.B., M.A., R.C., V.T., M.G., C.D.N., K.L.S., R.K., J.v.M., R.W.B., S.B., J.E.M. and M.K. Contributed reagents/materials: M.Z.C. and K.T.

#### SUPPLEMENTARY INFORMATION

Supplementary material for this article is available at
http://dmm.biologists.org/lookup/suppl/doi:10.1242/dmm.002527/-/DC1

Received 6 January 2009; Accepted 17 February 2009.

#### REFERENCES

**Antonellis, A., Ellsworth, R. E., Sambuughin, N., Puls, I., Abel, A., Lee-Lin, S.Q., Jordanova, A., Kremensky, I., Christodoulou, K., Middleton, L. T. et al.** (2003). Glycyl tRNA synthetase mutations in Charcot-Marie-Tooth disease type 2D and distal spinal muscular atrophy type V. *Am. J. Hum. Genet.* **72**, 1293-1299.

**Antonellis, A., Lee-Lin, S. Q., Wasterlain, A., Leo, P., Quezado, M., Goldfarb, L. G., Myung, K., Burgess, S., Fischbeck, K. H. and Green, E. D.** (2006). Functional analyses of glycyl-tRNA synthetase mutations suggest a key role for tRNA-charging enzymes in peripheral axons. *J. Neurosci.* **26**, 10397-10406.

**Banks, G. T., Kuta, A., Isaacs, A. M. and Fisher, E. M. C.** (2008). TDP-43 is a culprit in human neurodegeneration and not just an innocent bystander. *Mamm. Genome* **19**, 299-305.

**Bostock, H.** (2004). Nerve excitability studies: past, present, future? *Suppl. Clin. Neurophysiol.* **57**, 85-90.

**Cader, M. Z., Ren, J., James, P. A., Bird, L. E., Talbot, K. and Stammers, D. K.** (2007). Crystal structure of human wildtype and S581L-mutant glycyl-tRNA synthetase: an enzyme underlying distal spinal muscular atrophy. *FEBS Lett.* **581**, 2959-2964.

**Chihara, T., Luginbuhl, D. and Luo, L.** (2007). Cytoplasmic and mitochondrial protein translation in axonal and dendritic terminal arborization. *Nat. Neurosci.* **10**, 828-837.

**Del Bo, R., Locatelli, F., Corti, S., Scarlato, M., Ghezzi, S., Prelle, A., Fagiolari, G., Moggio, M., Carpo, M., Bresolin, N. et al.** (2006). Coexistence of CMT-2D and distal SMA-V phenotypes in an Italian family with a GARS gene mutation. *Neurology* **66**, 752-754.

**Dignam, S. S. and Dignam, J. D.** (1984). Glycyl- and alanyl-tRNA synthetases from Bombyx mori: purification and properties. *J. Biol. Chem.* **259**, 4043-4048.

**Dubourg, O., Azzedine, H., Yaou, R. B., Pouget, J., Barois, A., Meininger, V., Bouteiller, D., Ruberg, M., Brice, A. and LeGuern, E.** (2006). The G526R glycyl-tRNA synthetase gene mutation in distal hereditary motor neuropathy type V. *Neurology* **66**, 1721-1726.

**Edvardson, S., Shaag, A., Kolesnikova, O., Gomori, J. M., Tarassov, I., Einbinder, T., Saada, A. and Elpeleg, O.** (2007). Deleterious mutation in the mitochondrial arginyl-transfer RNA synthetase gene is associated with pontocerebellar hypoplasia. *Am. J. Hum. Genet.* **81**, 857-862.

**Giuditta, A., Kaplan, B. B., van Minnen, J., Alvarez, J. and Koenig, E.** (2002). Axonal and presynaptic protein synthesis: new insights into the biology of the neuron. *Trends Neurosci.* **25**, 400-404.

**Gorio, A., Carmignoto, G., Finesso, M., Polato, P. and Nunzi, M. G.** (1983). Muscle reinnervation. II. Sprouting, synapse formation and repression. *Neuroscience* **8**, 403-416.

**James, P. A., Cader, M. Z., Muntoni, F., Childs, A. M., Crow, Y. J. and Talbot, K.** (2006). Severe childhood SMA and axonal CMT due to anticodon binding domain mutations in the GARS gene. *Neurology* **67**, 1710-1712.

**Jia, J., Arif, A., Ray, P. S. and Fox, P. L.** (2008). WHEP domains direct noncanonical function of glutamyl-Prolyl tRNA synthetase in translational control of gene expression. *Mol. Cell* **29**, 679-690.

**Jordanova, A., Irobi, J., Thomas, F. P., Van Dijck, P., Meerschaert, K., Dewil, M., Dierick, I., Jacobs, A., De Vriendt, E., Guergueltcheva, V. et al.** (2006). Disrupted function and axonal distribution of mutant tyrosyl-tRNA synthetase in dominant intermediate Charcot-Marie-Tooth neuropathy. *Nat. Genet.* **38**, 197-202.

**Kieran, D. and Greensmith, L.** (2004). Inhibition of calpains, by treatment with leupeptin, improves motoneuron survival and muscle function in models of motoneuron degeneration. *Neuroscience* **125**, 427-439.

**Koltzenburg, M., Stucky, C. L. and Lewin, G. R.** (1997). Receptive properties of mouse sensory neurons innervating hairy skin. *J. Neurophysiol.* **78**, 1841-1850.

**Lee, J. W., Beebe, K., Nangle, L. A., Jang, J., Longo-Guess, C. M., Cook, S. A., Davisson, M. T., Sundberg, J. P., Schimmel, P. and Ackerman, S. L.** (2006). Editing-defective tRNA synthetase causes protein misfolding and neurodegeneration. *Nature* **443**, 50-55.

**Li, S., Finley, J., Liu, Z. J., Qiu, S. H., Chen, H., Luan, C. H., Carson, M., Tsao, J., Johnson, D., Lin, G. et al.** (2002). Crystal structure of the cytoskeleton-associated protein glycine-rich (CAP-Gly) domain. *J. Biol. Chem.* **277**, 48596-48601.

**Lin, A. C. and Holt, C. E.** (2007). Local translation and directional steering in axons. *EMBO J.* **26**, 3729-3736.

**Martin, N., Jaubert, J., Gounon, P., Salido, E., Haase, G., Szatanik, M. and Guenet, J. L.** (2002). A missense mutation in Tbce causes progressive motor neuronopathy in mice. *Nat. Genet.* **32**, 443-447.

**Maurer, K., Bostock, H. and Koltzenburg, M.** (2007). A rat *in vitro* model for the measurement of multiple excitability properties of cutaneous axons. *Clin. Neurophysiol.* **118**, 2402-2412.

**Mozhui, K., Ciobanu, D. C., Schikorski, T., Wang, X., Lu, L. and Williams, R. W.** (2008). Dissection of a QTL hotspot on mouse distal chromosome 1 that modulates neurobehavioral phenotypes and gene expression. *PLoS Genet.* **4**, e1000260.

**Nangle, L. A., Motta, C. M. and Schimmel, P.** (2006). Global effects of mistranslation from an editing defect in mammalian cells. *Chem. Biol.* **13**, 1091-1100.

**Nangle, L. A., Zhang, W., Xie, W., Yang, X. L. and Schimmel, P.** (2007). Charcot-Marie-Tooth disease-associated mutant tRNA synthetases linked to altered dimer interface and neurite distribution defect. *Proc. Natl. Acad. Sci. USA* **104**, 11239-11244.

**Nolan, P. M., Peters, J., Strivens, M., Rogers, D., Hagan, J., Spurr, N., Gray, I. C., Vizor, L., Brooker, D., Whitehill, E. et al.** (2000). A systematic, genome-wide, phenotype-driven mutagenesis programme for gene function studies in the mouse. *Nat. Genet.* **25**, 440-443.

**Park, S. G., Ewalt, K. L. and Kim, S.** (2005). Functional expansion of aminoacyl-tRNA synthetases and their interacting factors: new perspectives on housekeepers. *Trends Biochem. Sci.* **30**, 569-574.

**Park, S. G., Schimmel, P. and Kim, S.** (2008). Aminoacyl tRNA synthetases and their connections to disease. *Proc. Natl. Acad. Sci. USA* **105**, 11043-11049.

**Puls, I., Jonnakuty, C., LaMonte, B. H., Holzbaur, E. L., Tokito, M., Mann, E., Floeter, M. K., Bidus, K., Drayna, D., Oh, S. J. et al.** (2003). Mutant dynactin in motor neuron disease. *Nat. Genet.* **33**, 455-456.

**Ribas de Pouplana, L. and Geslain, R.** (2008). Not just because it is there: aminoacyl-tRNA synthetases gain control of the cell. *Mol. Cell* **30**, 3-4.

**Rogers, D. C., Fisher, E. M., Brown, S. D., Peters, J., Hunter, A. J. and Martin, J. E.** (1997). Behavioral and functional analysis of mouse phenotype: SHIRPA, a proposed protocol for comprehensive phenotype assessment. *Mamm. Genome* **8**, 711-713.

**Rogers, D. C., Peters, J., Martin, J. E., Ball, S., Nicholson, S. J., Witherden, A. S., Hafezparast, M., Latcham, J., Robinson, T. L., Quilter, C. A. et al.** (2001). SHIRPA: validation for longitudinal study of neurological dysfunction in mice. *Neurosci. Lett.* **306**, 89-92.

**Scheper, G. C., van der Klock, T., van Andel, R. J., van Berkel, C. G., Sissler, M., Smet, J., Muravina, T. I., Serkov, S. V., Uziel, G., Bugiani, M. et al.** (2007). Mitochondrial aspartyl-tRNA synthetase deficiency causes leukoencephalopathy with brain stem and spinal cord involvement and lactate elevation. *Nat. Genet.* **39**, 534-539.

**Schwarz, J. R., Glassmeier, G., Cooper, E. C., Kao, T. C., Nodera, H., Tabuena, D., Kaji, R. and Bostock, H.** (2006). KCNQ channels mediate IKs, a slow K+ current regulating excitability in the rat node of Ranvier. *J. Physiol.* **573**, 17-34.

**Seburn, K. L., Nangle, L. A., Cox, G. A., Schimmel, P. and Burgess, R. W.** (2006). An active dominant mutation of glycyl-tRNA synthetase causes neuropathy in a Charcot-Marie-Tooth 2D mouse model. *Neuron* **51**, 715-726.

**Sharp, P. S., Dick, J. R. and Greensmith, L.** (2005). The effect of peripheral nerve injury on disease progression in the SOD1(G93A) mouse model of amyotrophic lateral sclerosis. *Neuroscience* **130**, 897-910.

**Shiba, K., Schimmel, P., Motegi, H. and Noda, T.** (1994). Human glycyl-tRNA synthetase. Wide divergence of primary structure from bacterial counterpart and species-specific aminoacylation. *J. Biol. Chem.* **269**, 30049-30055.

**Sivakumar, K., Kyriakides, T., Puls, I., Nicholson, G. A., Funalot, B., Antonellis, A., Sambuughin, N., Christodoulou, K., Beggs, J. L., Zamba-Papanicolaou, E. et al.** (2005). Phenotypic spectrum of disorders associated with glycyl-tRNA synthetase mutations. *Brain* **128**, 2304-2314.

**Skre, H.** (1974). Genetic and clinical aspects of Charcot-Marie-Tooth's disease. *Clin. Genet.* **6**, 98-118.

**Tucci, V., Achilli, F., Blanco, G., Lad, H. V., Wells, S., Godinho, S. and Nolan, P. M.** (2007). Reaching and grasping phenotypes in the mouse (Mus musculus): a characterization of inbred strains and mutant lines. *Neuroscience* **147**, 573-582.

**Weisbrich, A., Honnappa, S., Jaussi, R., Okhrimenko, O., Frey, D., Jelesarov, I., Akhmanova, A. and Steinmetz, M. O.** (2007). Structure-function relationship of CAP-Gly domains. *Nat. Struct. Mol. Biol.* **14**, 959-967.

**Williams, J., Osvath, S., Khong, T. F., Pearse, M. and Power, D.** (1995). Cloning, sequencing and bacterial expression of human glycine tRNA synthetase. *Nucleic Acids Res.* **23**, 1307-1310.

**Xie, W., Nangle, L. A., Zhang, W., Schimmel, P. and Yang, X. L.** (2007). Long-range structural effects of a Charcot-Marie-Tooth disease-causing mutation in human glycyl-tRNA synthetase. *Proc. Natl. Acad. Sci. USA* **104**, 9976-9981.